RECTIWEATHER: PHOTO-REALISTIC ADVERSE WEATHER REMOVAL VIA ZERO-SHOT SOFT WEATHER PERCEPTION AND RECTIFIED FLOW

Anonymous authors
Paper under double-blind review

ABSTRACT

Despite significant progress in Adverse Weather Removal (AWR), challenges remain in applying existing methods to real-world scenarios and in generating photo-realistic and visually compelling outcomes. The limited generalization of current approaches can be attributed to their inability to accurately perceive complex degradations in weather-affected images. Moreover, owing to optimization objectives that prioritize distortion losses, discriminative methods often produce overly smooth reconstructions. To address these challenges, we propose **RectiWeather**, a novel AWR framework guided by zero-shot soft perceptions extracted from pre-trained vision–language models (VLMs). Specifically, we design an AWR-specific Question Answering (AWR-QA) module that guides VLMs to produce soft perceptions of weather conditions and low-level attributes. These soft perceptions are then integrated into baseline AWR models through attribute-modulated normalization (AMN) and weather-weighted adapters (WWA), enabling posterior mean estimation while minimizing distortion loss. Furthermore, we map the posterior output to the clean image distribution using a perception-aware rectified flow model, where soft perceptions define the source distribution and guide the velocity field. Extensive experiments show that RectiWeather consistently surpasses state-of-the-art baselines in fidelity and perceptual metrics across both all-in-one and out-of-distribution scenarios. Our code will be released upon publication.

1 INTRODUCTION

As a fundamental task in computer vision, Adverse Weather Removal (AWR) aims to restore weather-degraded images to clean counterparts, which is essential for emerging sectors such as autonomous driving (Zang et al., 2019). These weather degradations include, but are not limited to, rain (Li et al., 2019; Zhang et al., 2024), snow (Chen et al., 2021; Zhang et al., 2021), haze (Li et al., 2017; Cai et al., 2016; Li et al., 2020a; Song et al., 2023), and low light conditions (Zhou et al., 2024; 2025). To address these weather degradations, many works focus on networks targeting a single weather degradation (Zang et al., 2019; Li et al., 2019; Fu et al., 2017; Zhang et al., 2024; Li et al., 2017; Cai et al., 2016; Li et al., 2020a; Song et al., 2023), while only a few works have proposed non-blind general-purpose models designed to restore all weather conditions (Li et al., 2020b). However, these models typically depend on predefined priors or separate task-specific models for each type of weather degradation, making them less reliable in blind real-world scenarios. For improved efficacy, recent studies have increasingly focused on all-in-one blind restoration models (Valanarasu et al., 2022; Ye et al., 2023; Yang et al., 2024; Potlapalli et al., 2023; Luo et al., 2023a; Rajagopalan & Patel, 2025), designed to adaptively handle various weather conditions within a single network.

Early blind AWR methods primarily rely on traditional Convolutional Neural Networks (CNNs) (Li et al., 2020b; Zhu et al., 2023; Krizhevsky et al., 2012), which restore degraded images by learning spatial patterns and fine-grained features via convolutional operations. Transformers (Vaswani, 2017) have also been extensively studied for AWR (Potlapalli et al., 2023; Valanarasu et al., 2022; Sun et al., 2024; Wang et al., 2024; Cui et al., 2025), often outperforming traditional CNNs with their superior ability in capturing global dependencies. Diffusion-based approaches (Özdenizci & Legenstein, 2023; Luo et al., 2023a; Zheng et al., 2024) have also been shown to be highly effective in AWR via their

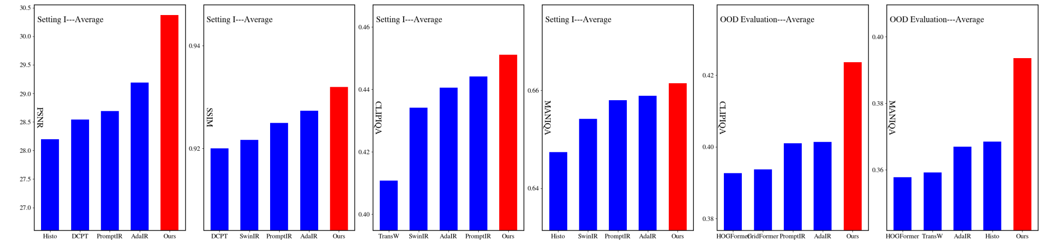

(a) Quantitative Comparisons

(b) Visual Comparisons on OOD evaluations.

Figure 1: RectiWeather significantly outperforms SOTA methods, especially on OOD data.

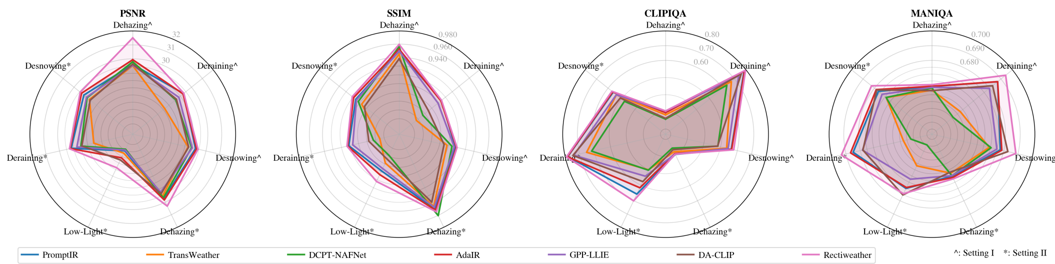

Figure 2: RectiWeather achieves the best performance on both fidelity and perceptual metrics.

iterative denoising process. Despite these advances, two challenges remain, hindering generalization in real-world scenarios and the generation of photo-realistic restorations.

First, a key open question is *how to reliably and accurately perceive the underlying weather condition from degraded inputs*. Essentially, such perception plays a pivotal role in the context of all-in-one AWR, as it allows the model to tailor its computational mechanisms or structural adaptations to produce weather-aware outputs with improved performance. To this end, several methods (Potlapalli et al., 2023; Valanarasu et al., 2022) incorporate learnable architectures to implicitly encode weather attributes (*e.g.*, type and severity) for guiding the restoration process, while others opt for explicit weather prediction by training or fine-tuning classifiers (Xu et al., 2024; Hu et al., 2025) or CLIP-based frameworks (Jiang et al., 2024; Luo et al., 2023a; Zeng et al., 2025). While promising within the training distribution, these methods exhibit noticeable performance drops on out-of-distribution (OOD) data, demonstrating their limited generalization ability.

Second, distortion-centric training in discriminative frameworks often leads to excessive smoothness, while diffusion-based methods, though perceptually compelling, commonly underperform in fidelity. *Achieving photo-realistic restorations with both minimal distortion and high perceptual quality remains largely unresolved in AWR*.

To address these limitations, we propose **RectiWeather**, an all-in-one AWR framework guided by zero-shot soft weather perceptions derived from pretrained Vision–Language Models (VLMs). **First**, within our developed AWR-specific Question Answering (AWR-QA) module, we craft explicit and unambiguous definitions to refine VLM understanding of weather conditions and low-level attributes, and then quantify their responses into soft perceptions. **Second**, we leverage these perceptions to modulate AWR backbones via Attribute-Modulated Normalization (AMN) and Weather-Weighted Adapters (WWA), enabling degradation-aware posterior estimation under distortion losses. **More importantly**, we introduce a perception-aware rectified flow that approximates the optimal transport map from a perception-dependent source distribution to the clean image distribution, enhancing photo-realism while maintaining competitive fidelity, as demonstrated in Fig. 1.

Our main contributions are: (1) We propose **RectiWeather**, an all-in-one AWR framework guided by **zero-shot** soft perceptions extracted from pretrained VLMs, and equipped with a perception-aware rectified flow to enhance photo-realism. (2) We introduce the AWR-QA module for extracting

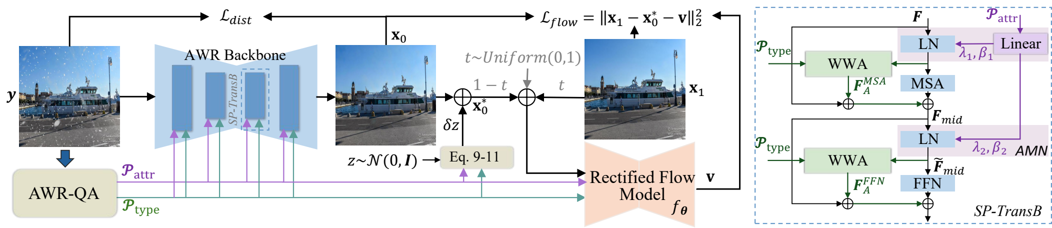

Figure 3: The framework of **RectiWeather**. With zero-shot soft perceptions ($\mathcal{P}_{type}$ and $\mathcal{P}_{attr}$) extracted from our developed AWR-QA, we introduce the Attribute-Modulated Normalization (AMN) and Weather-weighted Adapters (WWA) into AWR backbones to enhance fidelity. Subsequently, based on the posterior estimation $\mathbf{x}_0$, we develop a perception-aware rectified flow model f_θ, in which both the source distribution and the velocity field estimation are informed by soft perceptions, enabling photo-realistic restoration.

quantitative weather-aware soft perceptions, and AMN and WWA as **plug-and-play** components for degradation-aware posterior estimation, which improve fidelity and generalize across diverse AWR backbones. (3) We conduct extensive experiments showing that RectiWeather achieves state-of-the-art fidelity and perceptual performance on both in-distribution and out-of-distribution benchmarks.

2 METHOD

The key contributions of this work is to introduce zero-shot soft perceptions extracted from VLMs into AWR backbones for fidelity improvement, and to develop a perception-aware rectified flow model to enhance perceptual quality. The overall framework of our method is demonstrated in Fig. 3. Specifically, we first develop the AWR-related Question Answering module to acquire quantified soft perceptions of weather type and low-level visual attributes (Sec. 2.1). Then, we integrate extracted soft perceptions to assist existing AWR baselines via attribute-modulated normalization and weather-weighted adapters (Sec. 2.2). Furthermore, upon high-quality posterior estimation, we introduce a perceptual-aware rectified flow model to achieve the photo-realistic restoration (Sec. 2.3).

2.1 AWR-SPECIFIC QUESTION ANSWERING MODULE (AWR-QA)

Figure 4: Methods with implicit weather perception present limited weather perception capability on OOD data (R100L (Yang et al., 2017)), leading to poor restoration effect.

An all-in-one AWR agent should incorporate dedicated mechanisms for perceiving weather variations in input images, enabling adaptive decisions on model selection (Yang et al., 2024), architecture width (Xu et al., 2024), and computational flow (Potlapalli et al., 2023). Such specially designed modules can generally be divided into two categories: (1) Several approaches (*e.g.*, PromptIR (Potlapalli et al., 2023) and TransWeather Valanarasu et al. (2022)) employ learnable parameters to implicitly perceive weather type and severity; (2) Some recent methods (*e.g.*, DACLIP (Luo et al., 2023a) and DCPT (Hu et al., 2025)) pursue explicit weather classification through classifier training or CLIP-based fine-tuning, with classification accuracy reported to demonstrate their perception ability. Although effective on in-distribution samples, both implicit learnable modules and fine-tuned classifiers exhibit limited generalization to out-of-distribution (OOD) data, as presented in Fig. 4 and Table. 1. Notably, CLIP-based classifiers, despite originating from VLMs with remarkable zero-shot capacity, show reduced generalization after finetuning (see Table 1), as the adaptation enforces near-perfect classification on comparatively small training datasets.

Accordingly, to fully inherit the zero-shot strength of pretrained VLMs, we directly exploit their perceptual ability to acquire robust perceptions of weather conditions as well as critical visual attributes. Trained on massive image–text corpora, VLMs inherently possess the ability to assess input image quality. Recent studies (Wu et al., 2024; You et al., 2024) have further enhanced their perceptual and interpretive capacity through finetuning on large-scale visual instruction–response

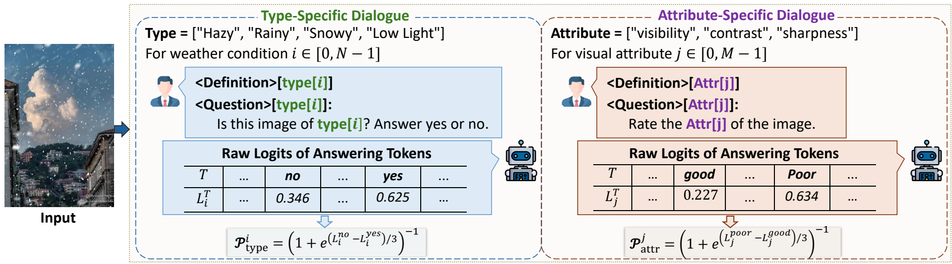

Figure 5: Our developed AWR-specific Question Answering Module.

datasets. While these VLMs exhibit notable success in assessing global image quality, their direct utilization for advancing AWR remains hindered by two critical challenges: (1) Quality perception does not guarantee awareness of weather conditions, thus VLMs demand additional guidance and instructional cues to perform nuanced differentiation of weather-corrupted images; (2) The reliance on one-hot labels for weather perception imposes severe limitations on handling multiple degradations. Yet, prevailing VLMs are trained with one-hot labels, leaving the acquisition of soft perceptions an open challenge. To address these issues, we develop an AWR-specific question answering module as presented in Fig. 5. Specifically, our AWR-QA involves two forms of conversation (type-specific and attribute-specific), and possesses the following distinctive characteristics.

Table 1: The accuracy comparison of weather condition prediction on setting I and OOD data. With our developed AWR-QA module, our pipeline demonstrates markedly improved performance. [Key: †: training or finetuning; "Only Question": Removing Definition from our AWR-QA].

Methods	*Setting I*				*OOD Data*			
	Hazy	*Rainy*	*Snowy*	*Average*	*Hazy*	*Rainy*	*Snowy*	*Average*
Original CLIP	96.70%	97.00%	33.61%	75.68%	91.14%	84.00%	19.48%	82.48%
Finetuning CLIP†	99.40%	99.50%	99.67%	99.50%	92.06%	82.00%	90.83%	91.71%
CLIP-Adapter†	99.80%	100%	100%	99.89%	81.58%	91.00%	91.49%	82.97%
DACLIP†	100%	100%	100%	100%	92.48%	93.00%	92.31%	92.47%
Only Question	95.20%	86.50%	82.70%	90.52%	93.20%	85.00%	81.83%	91.65%
AWR-QA	99.10%	91.50%	95.51%	97.06%	97.55%	96.00%	96.56%	97.40%

Definition-Question-Answering Process VLM conversations typically adopt the query–response pipeline: `<Img>` + `<Question>` → `<Answer>`. However, this pipeline is sub-optimal for AWR task, as evidenced by the low perception accuracy of snowy images in Table 1 ("Only Question"). This observation demonstrates that existing VLMs, while trained to perceive visual quality and degradation, lack explicit grounding in the causal origins of these degradations, making direct weather identification inherently ambiguous. Consequently, the perceptual similarity between snow and haze, both characterized by diminished contrast and visibility, results in frequent misclassification of snowy images as hazy when explicit priors are absent. To address this limitation, we propose to insert textual cues `<Definition>` for the weather condition between `<Img>` and `<Question>` to strengthen VLMs' ability to distinguish weather-induced degradations. By injecting `<Definition>` in AWR-QA, we constrain the decision boundary that VLMs otherwise learn only from quality cues, lowering the ambiguity among conditions sharing similar degradations and achieving higher weather condition prediction accuracy in Table 1.

Producing Soft Perceptions via Multiple Conservations To facilitate high-quality generalization in real-world scenarios with complex weather conditions (*e.g.*, rain+snow), we aim to produce soft perceptions instead of one-hot label by employing N independent type-specific conversations. In each conversation $i \in [0, N]$, the definition and question for weather type i (`<Definition>[type[i]]` and `<Question>[type[i]]`) are fed into VLMs and the probability corresponding to weather type i ($\mathcal{P}^i_{type}$) is quantified based on the raw logits of answering tokens. Specifically, the logits for token "`yes`" and "`no`" are utilized as anchors for positive and negative responses to the **Yes-or-No** `<Question>[type[i]]`, then the quantified probability $\mathcal{P}^i_{type}$ and the soft weather perception $\mathcal{P}_{type}$ can be calculated as:

$$\mathcal{P}_{type} = \{\mathcal{P}^i_{type}\}, \quad \mathcal{P}^i_{type} = (1 + e^{(L_i^{no} - L_i^{yes})/3})^{-1}, \quad i \in [0, N]. \tag{1}$$

Similarly, besides the type-specific conversations, M attribute-specific dialogues are deployed to perceive low-level attributes for inputs. Specifically, as the the `<Question>[Attr[j]]` is essentially a **How** question, we leverage the logits for token "`good`" and "`poor`" as anchors, and calculate

Table 2: Comparison with SOTA methods on all-in-one image restoration (setting I). [Key: Best; Second-best; Third-best].

Task	Metrics	CNN-based WGWS-Net	CNN-based DCPT-NAFNet	Transformer-based SwinIR	Transformer-based PromptIR	Transformer-based TransWeather	Transformer-based Histoformer	Transformer-based GridFormer	Transformer-based AdaIR	Transformer-based HOGFormer	SDE/Diffusion-based DACLIP	SDE/Diffusion-based GPPLLIE	SDE/Diffusion-based UniRestore	Our RectiWeather
Dehazing	PSNR↑	25.2422	29.5123	28.1335	29.0742	28.8708	28.8753	29.7015	29.8552	26.2312	29.1248	28.9203	24.1892	31.8040
	SSIM↑	0.9198	0.9561	0.9490	0.9492	0.9449	0.9532	0.9550	0.9523	0.9446	0.9366	0.9498	0.8272	0.9595
	LPIPS↓	0.0915	0.0245	0.0351	0.0302	0.0327	0.0284	0.0249	0.0290	0.0361	0.0249	0.0336	0.1008	0.0236
	FID↓	13.9170	6.6464	10.5504	8.5657	9.6171	8.1998	5.4800	8.2878	9.7512	5.6563	9.3160	19.1667	4.1463
	MUSIQ↑	52.3578	56.1662	55.9391	55.9365	56.0669	56.1384	56.2397	55.9506	56.0219	56.871	55.8657	54.7502	57.1226
	CLIPIQA↑	0.2506	0.2580	0.2944	0.3046	0.2831	0.2591	0.2616	0.2957	0.2557	0.2623	0.3045	0.2530	0.3055
	NIQE↓	4.3388	4.0909	3.9766	3.9844	3.8393	4.0926	3.9909	4.0457	4.1116	3.8933	3.9641	4.4329	3.6223
	MANIQA↑	0.6277	0.6398	0.6390	0.6420	0.6367	0.6379	0.6416	0.6423	0.6359	0.6360	0.6408	0.6087	0.6446
Deraining	PSNR↑	25.4435	26.6555	28.1922	28.2102	24.3043	27.2624	26.9545	28.2166	25.9042	26.8019	27.3112	21.8189	28.3725
	SSIM↑	0.8057	0.8340	0.8870	0.8881	0.8151	0.8551	0.8397	0.8868	0.8226	0.8504	0.8784	0.6732	0.8886
	LPIPS↓	0.1922	0.1536	0.0748	0.0739	0.1365	0.1331	0.1066	0.0738	0.1626	0.0776	0.0967	0.2254	0.0570
	FID↓	42.6285	54.8526	25.3864	25.9583	50.3034	44.4640	34.9925	25.4323	57.4706	29.3110	30.4662	67.9509	21.6385
	MUSIQ↑	63.9255	64.9781	70.4030	70.7116	68.8380	67.7278	68.7697	70.5658	66.0232	70.3025	70.2249	64.6621	70.8914
	CLIPIQA↑	0.6303	0.6326	0.7695	0.7827	0.6721	0.6856	0.7025	0.7871	0.6623	0.7589	0.7359	0.6585	0.7962
	NIQE↓	3.5515	3.5908	3.6381	3.6483	3.7658	3.4542	3.4429	3.5867	3.3721	3.1197	3.5928	4.5751	3.1935
	MANIQA↑	0.6208	0.6119	0.6859	0.6871	0.6253	0.6417	0.6383	0.6871	0.6149	0.6827	0.6798	0.6135	0.6941
Desnowing	PSNR↑	26.2841	27.5454	27.4389	28.2108	26.9457	27.3890	27.5816	28.4096	26.2566	27.0387	27.6699	21.8825	28.6361
	SSIM↑	0.8330	0.8886	0.8874	0.8966	0.8769	0.8870	0.8890	0.8992	0.8794	0.8701	0.8938	0.6402	0.9005
	LPIPS↓	0.1145	0.0808	0.0705	0.0627	0.0790	0.0846	0.0734	0.0590	0.0886	0.0677	0.0668	0.1145	0.0537
	FID↓	27.2584	29.1007	25.1864	22.1090	29.7221	30.7080	23.6043	20.8006	32.8779	23.4294	25.3291	40.0907	17.2547
	MUSIQ↑	69.0165	69.7187	68.6227	69.1966	69.1384	70.1404	69.1025	69.2825	69.0672	70.6822	69.4237	68.5674	70.4982
	CLIPIQA↑	0.4787	0.4836	0.5552	0.5638	0.5362	0.4947	0.5017	0.5663	0.4864	0.4819	0.5452	0.4484	0.5784
	NIQE↓	3.1464	3.0592	2.8550	2.9555	2.9998	3.1293	2.8889	2.9380	3.0156	2.9284	3.0459	3.3874	2.6762
	MANIQA↑	0.6645	0.6611	0.6688	0.6749	0.6584	0.6651	0.6681	0.6771	0.6601	0.6829	0.6698	0.6356	0.6885
Average	PSNR↑	25.6122	28.5387	27.9082	28.6901	27.7213	28.2002	28.6890	29.1908	26.2034	28.1707	28.3243	23.1562	30.3658
	SSIM↑	0.8782	0.9200	0.9216	0.9249	0.9078	0.9202	0.9202	0.9273	0.9093	0.9048	0.9232	0.7477	0.9319
	LPIPS↓	0.1104	0.0576	0.0513	0.0459	0.0597	0.0588	0.0502	0.0440	0.0677	0.0450	0.0517	0.1192	0.0374
	FID↓	21.5575	19.4927	17.0820	15.0166	20.8444	19.7380	14.8055	14.3673	22.7679	14.2141	17.0083	31.5666	10.4631
	MUSIQ↑	59.2015	61.6673	61.7779	62.0022	61.8471	62.0979	61.9235	62.0225	61.4858	62.9714	61.9846	60.4618	63.1151
	CLIPIQA↑	0.3689	0.3749	0.4342	0.4442	0.4108	0.3851	0.3907	0.4406	0.3778	0.3907	0.4327	0.3632	0.4511
	NIQE↓	3.8535	3.6911	3.5647	3.6037	3.5510	3.7002	3.5623	3.6251	3.6637	3.4854	3.6165	4.0998	3.2590
	MANIQA↑	0.6392	0.6438	0.6542	0.6580	0.6427	0.6474	0.6501	0.6589	0.6416	0.6568	0.6548	0.6182	0.6647

the attribute perception $\mathcal{P}_{attr}$ as:

$$\mathcal{P}_{attr} = \{\mathcal{P}^j_{attr}\}, \quad \mathcal{P}^j_{attr} = (1 + e^{(L_i^{poor} - L_i^{good})/3})^{-1}, \quad j \in [0, M]. \tag{2}$$

Therefore, with our soft weather and attribute perceptions, $\mathcal{P}_{type}$ tends to produce a non-sharp distribution under unseen weather conditions, facilitating expert mixing behavior, while $\mathcal{P}_{attr}$ directly encodes low-level degradation intensity, alleviating error propagation from weather misclassification.

Remarkable Zero-shot Capability of AWR-QA To evaluate the effectiveness of our developed AWR-QA, we convert soft weather perceptions into one-hot labels and compare the statistical accuracy against existing methods in Table 1. Though training or finetuning CLIP-based approaches achieves slightly higher performance, their performance drop heavily on OOD data while our AWR-QA is capable of achieve consistent perceptions across various weather conditions.

2.2 Enhancing AWR Baselines using Weather Perceptions

With robust weather and visual attribute perceptions extracted from VLMs, we aim to enhance various baseline models using $\mathcal{P}_{type}$ and $\mathcal{P}_{attr}$ in this section. As presented in Fig. 3, we take transformer-based baselines as the example for illustration. Overall, two additional layers are introduced into the Soft Perceptions guided Transformer Block (SP-TransB).

Attributed-Modulated Normalization (AMN) The attribute perception is integrated to modulate the layer normalization. Specifically, given an input feature $\mathbf{F}$ or $\mathbf{F}_{mid}$, AMN modulate its output of standard layer normalization with the scale and bias, which are learned from $\mathcal{P}_{attr}$ via linear operation. This design allows the adaptive modulate magnitude based on low-level attribute perception and alleviates the error propagation when the weather perception is not accurate in extremely complex scenarios. The calculation process of AMN can be represented as:

$$\lambda_1, \beta_1, \lambda_2, \beta_2 = \text{Linear}(\mathcal{P}_{attr}), \tag{3}$$

$$\tilde{\mathbf{F}} = \lambda_1 \odot \text{LN}(\mathbf{F}) + \beta_1, \quad \tilde{\mathbf{F}}_{mid} = \lambda_2 \odot \text{LN}(\mathbf{F}_{mid}) + \beta_2. \tag{4}$$

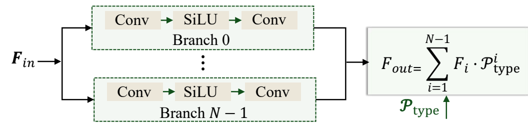

Figure 6: Soft weather perceptions $\mathcal{P}_{type}$ serve as branch weight in our developed WW-Adapter.

Weather-Weighted Adapters (WW-Adapter) To achieve weather-aware modeling, we incorporate soft weather perceptions $\mathcal{P}_{type}$ by developing the WW-Adapter alongside the MSA and FFN components. The details of WW-Adapter is shown in Fig. 6. Specifically, the WW-Adapter module contains N branches, with each corresponding to one weather type. The output of WW-Adapter is calculated as the weighted sum of the output of each branch:

$$\mathbf{F}_{out} = \sum_{i=0}^{N-1} \mathbf{F}_i \cdot \mathcal{P}^i_{\text{type}}, \quad \mathbf{F}_i = [\text{Conv}, \text{SiLU}, \text{Conv}]^i(\mathbf{F}_{in}). \tag{5}$$

Therefore, the calculation of SP-TransB can be formulated as:

$$\tilde{\mathbf{F}} = \text{AMN}(\mathbf{F}), \quad \mathbf{F}_A^{MSA} = \text{WWA}(\tilde{\mathbf{F}}, \mathcal{P}_{type}), \quad \mathbf{F}_m = \mathbf{F} + \text{MSA}(\tilde{\mathbf{F}}) + \alpha_A^{MSA} \cdot \mathbf{F}_A^{MSA}, \tag{6}$$

$$\tilde{\mathbf{F}}_m = \text{AMN}(\mathbf{F}_m), \mathbf{F}_A^{FFN} = \text{WWA}(\tilde{\mathbf{F}}_m, \mathcal{P}_{type}), \quad \mathbf{F}' = \mathbf{F}_m + \text{FFN}(\tilde{\mathbf{F}}_m) + \alpha_A^{FFN} \cdot \mathbf{F}_A^{FFN}, \tag{7}$$

where α_A^{MSA} and α_A^{FFN} are two learnable coefficients for adaptively adjusting the strength of weather-weighted adapters. Following TransWeather (Valanarasu et al., 2022), the optimization of AWR backbones with SP-TransB is achieved by minimizing the following distortion loss $\mathcal{L}_{dist}$:

$$\mathcal{L}_{dist} = \mathcal{L}_1(\mathbf{x}_1, \mathbf{x}_0) + 0.04 \times \mathcal{L}_{percep}(\mathbf{x}_1, \mathbf{x}_0), \tag{8}$$

where $\mathbf{x}_1$ and $\mathbf{x}_0$ denote the clean image and posterior output of AWR backbones with SP-TransB.

2.3 Weather-aware Rectified Flow

Using soft weather cues as conditioning, attribute-modulated normalization together with weather-weighted adapters consistently improves fidelity metrics over the corresponding AWR backbones. Nevertheless, the posterior estimate $\mathbf{x}_0$ exhibits over-smoothing and lacks photorealism. We therefore learn a weather-aware rectified flow to map the posterior-estimate distribution to the clean-image distribution, which differs from the original RF process (Liu et al., 2022) in the following aspects.

Parameterizing Source Distribution using Soft Perceptions RF approximates a straight-path flow that effects a distributional transport from source to target. In our setting, the target distribution is the clean-image distribution, from which clean images $\mathbf{x}_1$ are sampled. However, the choice of source distribution and its sampling scheme merits careful investigation. The standard RF, trained from Gaussian noise to natural images, is effective for generation yet underperforms in AWR owing to limited data-consistency. A similar limitation arises in approaches that take the degraded observation $\mathbf{y}$ as the source for flow learning (Albergo & Vanden-Eijnden, 2022). PMRF (Ohayon et al., 2024) defines the source by perturbing posterior estimates with random noise and demonstrates efficacy on face restoration, denoising, and super-resolution. This stochastic perturbation mitigates singularities inherent to learning a strictly deterministic mapping between source and target. Given the adverse impact of noise on fidelity, PMRF employs modest, task-dependent noise magnitudes, indicating that a constant noise level is ill-suited to AWR. To this end, we propose to parameterize the source distribution exclusively through soft perceptions extracted by our AWR-QA.

Concretely, we first compute a normalized entropy H for weather perceptions $\mathcal{P}_{type} \in \mathbb{R}^N$, and aggregate attribute perceptions $\mathcal{P}_{attr} \in \mathbb{R}^M$ into a scalar degradation severity indicator. We then We then fuse type-uncertainty and attribute-severity and calculate a scalar perturbation scale within a prescribed range $[\delta_{min}, \delta_{max}]$. The overall process can be summarized as:

$$\tilde{\mathcal{P}}_{type} = \frac{\mathcal{P}_{type}}{\sum_{i=0}^{N-1} \mathcal{P}^i_{type}}, \quad H = -\frac{\sum_{i=0}^{N-1} \mathcal{P}^i_{type} \log \mathcal{P}^i_{type}}{\log N}, \quad s_{attr} = 1 - \frac{\sum_{i=0}^{M-1} \mathcal{P}^i_{attr}}{M}, \tag{9}$$

$$u = \alpha H + (1-\alpha) s_{attr}, \quad \delta = \delta_{min} + (\delta_{max} - \delta_{min}) u, \tag{10}$$

where α is set to 0.5 to control the trade-off between weather uncertainty and attribute severity.δ_{min} and δ_{max} are 0.025 and 0.1, respectively. Therefore, as presented in Eq. 11, the source distribution in our weather-aware rectified flow is isotropic Gaussian centered at posterior estimate $\mathbf{x}_o$ and parameterized by a VLM-driven perceptions, ensuring data-consistent yet adaptive randomness.

$$p_0^* = \mathcal{N}(\mathbf{x}_0, \delta^2 I), \quad \mathbf{x}_0^* = \mathbf{x}_0 + \delta z, \quad z \sim \mathcal{N}(0, I). \tag{11}$$

Figure 7: Visual comparisons on setting I. Our RectiWeather is capable of preserving fine details and maintaining perceptual quality.

Table 3: Our extracted soft degradation perceptions consistently achieves remarkable improvements for CNN or Transformer networks on setting I.

Methods	*Dehazing*		*Deraining*		*Desnowing*		*Average*	
	PSNR ↑	SSIM ↑	PSNR ↑	SSIM ↑	PSNR ↑	SSIM ↑	PSNR ↑	SSIM ↑
NAFNet	29.2794	0.9481	26.0314	0.8494	28.1914	0.8953	28.5554	0.9195
NAFNet+Prior (Ours)	31.3548	0.9572	26.5934	0.8617	28.6328	0.8982	30.0240	0.9269
TransWeather	28.8708	0.9449	24.3043	0.8151	26.9457	0.8769	27.7213	0.9078
TransWeather+Prior (Ours)	30.7832	0.9574	26.3847	0.8557	28.1937	0.8943	29.4306	0.9251
SwinIR	28.133	0.9490	28.1922	0.8870	27.4389	0.8873	27.9082	0.9216
SwinIR+Prior (Ours)	29.2637	0.9542	28.3142	0.8881	27.8045	0.8891	28.6713	0.9251
PromptIR	29.0742	0.9492	28.2102	0.8881	28.2108	0.8966	28.6901	0.9249
PromptIR+Prior (Ours)	30.1556	0.9530	27.9903	0.8863	28.6774	0.9034	29.4219	0.9291
Histoformer	28.8753	0.9532	27.2624	0.8551	27.3890	0.8870	28.2002	0.9202
Histoformer+Prior (Ours)	29.8024	0.9625	27.6263	0.8612	27.9804	0.8938	28.9527	0.9283
AdaIR	29.8552	0.9523	28.2166	0.8868	28.4096	0.8992	29.1908	0.9273
AdaIR+Prior (Ours)	31.9523	0.9614	28.5753	0.8892	28.7732	0.9009	30.5164	0.9332

Perception-aware Velocity Field Estimation Based on the source distribution p_0^* and its samples $\mathbf{x}_0^*$, we train a perception-aware rectified flow model f_θ via the following optimization:

$$\arg\min_{\theta} \int_0^1 \mathbb{E}\left[|| (\mathbf{x}_1 - \mathbf{x}_0^*) - f_\theta(\mathbf{x}_t^*, t, \mathcal{P}_{type}, \mathcal{P}_{attr}) ||^2 \right] dt, \tag{12}$$

where t is sampled from a uniform distribution $\mathcal{U}(0,1)$, $\mathbf{x}_t^* = t\mathbf{x}_1 + (1-t)\mathbf{x}_0^*$. More importantly, other than learning a unified velocity path for all weather-corrupted inputs, we incorporate soft perceptions into f_θ to achieve perception-aware velocity field estimation. Overall, AdaIR (Cui et al., 2025) is deployed as the backbone of f_θ, weather perceptions $\mathcal{P}_{type}$ is introduced via weather-weighted adapters. Moreover, the normalization coefficients of AMN in Eq. 4 is calculated upon the concatenation of timestep t and weather perceptions $\mathcal{P}_{attr}$.

3 Experiments

Experiment Settings and Datasets We evaluate RectiWeather under two all-in-one experimental settings. Setting I involves three core weather degradation tasks, dehazing, deraining, and desnowing, trained on a unified dataset comprising Reside-6K (Li et al., 2018), Rain100H (Yang et al., 2017), and Snow100K-L(Liu et al., 2018). Setting II further introduces the low-light enhancement task, with LOLv2-Real (Yang et al., 2021) included as an additional domain. To assess cross-domain robustness,

Table 4: Comparison with OOD data using weights pre-trained on setting I. [Key: Best; Second-best; Third-best].

Tasks	Metrics	Baselines						Ours
		PromptIR	TransWeather	Histoformer	GridFormer	AdaIR	HOGFormer	**RectiWeather**
Dehazing	MUSIQ↑	51.4000	51.9740	52.7529	54.6239	54.5125	52.8634	57.2632
	CLIPIQA↑	0.3677	0.3615	0.3642	0.3659	0.3677	0.3594	0.3921
	NIQE↓	5.3796	5.1483	4.8733	4.9918	4.9563	5.0271	4.4625
	MANIQA↑	0.2893	0.3079	0.3164	0.3209	0.3135	0.3029	0.3426
Deraining	MUSIQ↑	71.0463	70.4322	70.6811	70.6135	71.2161	70.2886	71.6847
	CLIPIQA↑	0.7526	0.7242	0.7156	0.7388	0.7570	0.7229	0.7689
	NIQE↓	3.3537	3.4932	3.8112	3.5161	3.3245	3.4784	2.9683
	MANIQA↑	0.6978	0.6628	0.6868	0.6866	0.6984	0.6852	0.7065
Desnowing	MUSIQ↑	70.4422	70.3448	71.1404	70.1392	70.4569	70.5921	71.3847
	CLIPIQA↑	0.5793	0.5227	0.5333	0.5336	0.5815	0.5742	0.5898
	NIQE↓	2.9182	3.1424	2.9812	3.0258	2.9156	2.9046	2.8125
	MANIQA↑	0.6897	0.6724	0.6850	0.6749	0.6915	0.6923	0.7033
Average	MUSIQ↑	54.1020	54.5709	55.3413	56.8251	56.7800	55.3619	59.2641
	CLIPIQA↑	0.4010	0.3883	0.3917	0.3937	0.4014	0.3927	0.4236
	NIQE↓	5.0405	4.8719	4.6225	4.7238	4.6761	4.7387	4.2325
	MANIQA↑	0.3460	0.3592	0.3685	0.3711	0.3670	0.3578	0.3936

we conduct out-of-distribution evaluations by testing models trained in Setting I on RTTS (Li et al., 2018), Rain100L(Yang et al., 2017), and Snow100K-S(Liu et al., 2018), each representing unseen test conditions for dehazing, deraining, and desnowing respectively.

Implementations Details Using Eq. 8, we first train the AWR baseline model (AdaIR (Cui et al., 2025)) with AMN and WWA on our combined dataset for 200 epochs. The initial learning rate is set to 2×10^{-4} and it is reduced to 10^{-7} by the end of training. Each training input is cropped into 192×192, and the batch size is set to 4. We use horizontal flips and rotations for data augmentation. We then optimize f_θ using Eq. 12 for 500 epochs, while other configurations keep unchanged. As in (Ohayon et al., 2024), we sample t uniformly from $U[0, 1]$ using a stratified sampling strategy. In the inference stage, the number of flow steps K is set to 5 in this work.

Compared Baselines and Metrics We benchmark our method against state-of-the-art (SOTA) approaches in all-in-one image restoration tasks including CNN-based methods (NAFNet (Chen et al., 2022), WGWS-Net (Zhu et al., 2023), DCPT-NAFNet (Hu et al., 2025)), Transformer-based methods (SwinIR (Liang et al., 2021), PromptIR (Potlapalli et al., 2023), TransWeather (Valanarasu et al., 2022), Histoformer (Sun et al., 2024), GridFormer (Wang et al., 2024), AdaIR (Cui et al., 2025), HOGFormer ()), and SDE/Diffusion-based methods (DACLIP (Luo et al., 2023a), GPPLLIE (Zhou et al., 2025), and UniRestore (Chen et al., 2025)). To test the efficacy of our method against these approaches, we compare performance across dehazing, deraining, desnowing, and low-light conditions across in and out-of-distribution settings, using fidelity (PSNR, SSIM (Wang et al., 2004)) and perceptual metrics (LPIPS (Zhang et al., 2018), FID (Heusel et al., 2017), MUSIQ (Ke et al., 2021), CLIPIQA (Wang et al., 2023), NIQE (Mittal et al., 2012), MANIQA (Yang et al., 2022)).

Quantitative Comparisons with Baselines Tab. 2 summarizes the quantitative comparisons between our method and current SOTA methods on setting I. Our method achieves superior performance on all three tasks, highlighting its advantage. Notably, the PSNR of our method surpasses the best SOTA by 1.17 dB on average. Moreover, our perceptual metrics significantly outperform the CNN-based and Transformer-based baselines, with only a few metrics slightly below DACLIP, a generative approach that requires numerous inference steps. These fidelity results demonstrate the effectiveness of the soft perceptions extracted from VLMs and of our designed AMN and WWA modules, while the exceptional perceptual quality corroborates the importance of our perception-aware rectified-flow model. See Tab. 5 for quantitative comparisons on Setting II, where RectiWeather also achieves the best performance on both fidelity and perceptual metrics. To demonstrate the plug-and-play nature of our perceptions, we integrate them into diverse baselines and achieve consistent gains on weather removal tasks (Tab. 3).

Visual Comparisons with Bselines Fig. 7 provides visual comparisons between our method and AWR baselines. For the hazy scenes (rows 1–2), SwinIR, PromptIR, and DCPT leave residual haze

Table 5: Comparison with SOTA methods on all-in-one image restoration (setting II). [Key: Best; Second-best; Third-best].

Tasks	Metrics	CNN-based		Transformer-based							SDE/Diffusion-based			**Our**
		NAFNet	DCPT-NAFNet	SwinIR	PromptIR	TransWeather	Histoformer	GridFormer	AdaIR	HOGFormer	DACLIP	GPP-LLIE	UniRestore	**RectiWeather**
Dehazing	PSNR↑	29.4842	29.2242	26.3268	29.3953	28.8925	27.2265	27.0659	29.6063	27.0072	28.4270	28.1868	24.1414	30.3797
	SSIM↑	0.9509	0.9604	0.9389	0.9497	0.9448	0.9418	0.9535	0.9512	0.9493	0.9365	0.9462	0.8346	0.9539
	LPIPS↓	0.0291	0.0246	0.0444	0.0294	0.0330	0.0339	0.0260	0.0296	0.0337	0.0272	0.0368	0.0952	0.0253
	FID↓	8.1313	6.9793	13.8706	8.4712	9.5456	10.1239	6.8404	8.3922	9.0061	6.2342	9.9210	18.5698	5.5366
	MUSIQ↑	55.9530	56.1014	56.3110	55.8436	55.9373	55.6795	56.1424	55.9427	55.8376	56.8943	55.6146	56.3163	56.7342
	CLIPIQA↑	0.2853	0.2598	0.2939	0.3002	0.2832	0.2561	0.2630	0.2950	0.2604	0.2700	0.2987	0.2659	0.2986
	NIQE↓	4.0587	4.0638	3.8112	3.9647	3.8340	4.0335	3.9798	4.0271	4.1015	3.8247	3.9758	4.4224	3.9401
	MANIQA↑	0.6416	0.6396	0.6386	0.6403	0.6356	0.6322	0.6392	0.6424	0.6415	0.6338	0.6394	0.6213	0.6445
Low-light	PSNR↑	18.6269	20.2516	16.1077	20.5389	20.9644	17.4699	19.9056	21.8332	19.9568	22.2302	20.3946	19.6627	23.6634
	SSIM↑	0.8383	0.8183	0.7913	0.8575	0.8377	0.7956	0.8112	0.8669	0.8318	0.8279	0.8517	0.7387	0.8842
	LPIPS↓	0.1153	0.1887	0.1384	0.0867	0.1176	0.1995	0.1249	0.0849	0.1676	0.1151	0.1157	0.1714	0.0644
	FID↓	43.3469	68.5468	62.8596	33.1933	46.6892	73.0903	49.2181	34.4985	57.8767	47.1134	43.2211	71.6247	29.3878
	MUSIQ↑	70.4247	55.9111	69.2740	68.9156	66.8728	58.9973	65.7178	68.9272	60.1414	69.1371	68.6057	66.7391	69.5077
	CLIPIQA↑	0.5366	0.4023	0.5277	0.5571	0.4001	0.4297	0.4743	0.5162	0.3446	0.4763	0.4415	0.4795	0.6010
	NIQE↓	4.3401	3.9823	4.3985	4.5524	3.9808	3.8475	4.4756	4.5544	3.8952	4.9906	3.8835	4.6244	3.9343
	MANIQA↑	0.6575	0.5897	0.6358	0.6601	0.6236	0.5912	0.6210	0.6587	0.5984	0.6706	0.6452	0.6328	0.6687
Deraining	PSNR↑	25.4421	26.3477	26.7710	27.9980	24.1490	25.5034	25.7722	28.1874	26.3770	26.1871	27.0394	21.6014	28.3006
	SSIM↑	0.8456	0.8253	0.8580	0.8829	0.8101	0.8069	0.8063	0.8857	0.8346	0.8360	0.8737	0.6743	0.8871
	LPIPS↓	0.1126	0.1648	0.1064	0.0755	0.1428	0.1881	0.1470	0.0733	0.1560	0.0876	0.1017	0.2255	0.0647
	FID↓	39.5993	58.2514	36.7157	27.1002	51.7666	62.6183	45.6402	25.8660	55.5853	32.7593	31.7345	69.8020	19.4836
	MUSIQ↑	70.0800	64.5522	69.4326	70.4612	68.4701	65.4731	66.8084	70.6815	65.9262	69.9443	70.0148	65.8471	71.1827
	CLIPIQA↑	0.7535	0.6158	0.7252	0.7829	0.6509	0.6393	0.6726	0.7856	0.6749	0.7466	0.7402	0.6629	0.7915
	NIQE↓	3.6333	3.6589	3.6001	3.5691	3.7411	3.2971	3.5996	3.6318	3.3972	3.1016	3.6051	3.6589	3.2237
	MANIQA↑	0.6707	0.6042	0.6650	0.6850	0.6153	0.5982	0.6150	0.6868	0.6191	0.6761	0.6767	0.6199	0.6932
Desnowing	PSNR↑	28.2893	27.2178	26.1904	27.9105	26.7268	26.5015	26.4140	28.4000	26.7946	26.5609	27.3473	21.8470	28.6734
	SSIM↑	0.8966	0.8843	0.8697	0.8919	0.8743	0.8698	0.8739	0.8981	0.8801	0.8661	0.8895	0.6415	0.9019
	LPIPS↓	0.0625	0.0857	0.0935	0.0665	0.0813	0.1057	0.0945	0.0608	0.0897	0.0731	0.0705	0.1819	0.0527
	FID↓	21.4393	30.7876	34.3009	22.9940	30.7250	36.8774	29.5384	21.1764	33.3173	25.8008	26.4275	45.5577	18.0723
	MUSIQ↑	69.5727	69.5594	67.9504	68.8747	69.1820	69.3072	68.2443	69.1902	69.1780	70.3695	69.0375	68.8181	70.6482
	CLIPIQA↑	0.5652	0.4776	0.5423	0.5621	0.5379	0.4762	0.4991	0.5655	0.4839	0.5082	0.5383	0.4556	0.5711
	NIQE↓	2.9698	3.0606	2.9673	2.8967	2.9637	3.2416	2.9067	2.9322	3.0508	2.8812	3.0507	3.0606	2.8239
	MANIQA↑	0.6760	0.6583	0.6568	0.6726	0.6580	0.6568	0.6595	0.6767	0.6581	0.6758	0.6658	0.6382	0.6826
Average	PSNR↑	28.1100	27.8153	25.7928	28.3130	27.2917	26.3028	26.3470	28.6668	26.5028	27.2754	27.3908	22.9132	29.2682
	SSIM↑	0.9167	0.9147	0.9007	0.9195	0.9027	0.8972	0.9054	0.9231	0.9092	0.8980	0.9157	0.7516	0.9268
	LPIPS↓	0.0530	0.0673	0.0714	0.0490	0.0643	0.0815	0.0656	0.0470	0.0713	0.0527	0.0584	0.1403	0.0402
	FID↓	17.5018	23.1392	25.3101	16.3230	22.6373	27.4171	24.1633	15.6456	26.3276	17.3612	19.1862	35.2829	12.2218
	MUSIQ↑	62.5064	61.2352	62.0532	62.1889	62.0184	61.1928	61.3430	62.3646	61.1712	63.1715	62.0566	61.8197	63.3251
	CLIPIQA↑	0.4363	0.3736	0.4301	0.4473	0.4086	0.3751	0.3919	0.4438	0.3791	0.4063	0.4284	0.3789	0.4525
	NIQE↓	3.6845	3.6998	3.5531	3.6163	3.5568	3.6959	3.6266	3.6671	3.6844	3.5117	3.6395	3.9222	3.5115
	MANIQA↑	0.6564	0.6392	0.6470	0.6563	0.6399	0.6342	0.6421	0.6588	0.6429	0.6535	0.6520	0.6271	0.6629

or introduce color distortion, as indicated by the red arrows. In contrast, our RectiWeather produces clearer and more natural results, closely resembling the ground truth. For the deraining case (row 3), competing methods fail to fully remove rain streaks or generate noticeable artifacts (orange arrows), whereas RectiWeather removes rain effectively while preserving fine structural details. In the desnowing case (row 4), other baselines fail to eliminate snowy particles and tend to blur background structures (black arrows). By comparison, RectiWeather yields sharper contours and more faithful textures, demonstrating its robustness across diverse weather degradations.

4 Conclusions

In this work, We introduce RectiWeather for adverse weather removal. By leveraging VLM-guided soft perceptions for restoration models, RectiWeather enhances the AWR baselines' awareness and adaptability to complex weather degradations without requiring additional supervision. Furthermore, with improved posterior estimation through perception-aware rectified flow, our method achieves significant performance in both all-in-one and out-of-distribution scenarios. Extensive experiments demonstrate RectiWeather's state-of-the-art performance in fidelity and perceptual quality.

Limitations Although RectiWeather handles complex weather conditions better than baseline models, its performance remains limited when image degradation (*e.g.*, the haze pattern) differs substantially from those seen during training. In addition, while our method is more efficient than full diffusion-based approaches such as DACLIP, the incorporation of VLM perception in the adverse-weather removal (AWR) backbone and rectified-flow procedure introduce a modest runtime overhead; for a 1024×1024 image, processing typically requires 0.4 s of additional time on a single 5090 GPU.

5 REPRODUCIBILITY STATEMENT

We have made significant efforts to ensure the reproducibility of our results. The main text provides complete details of the proposed framework (Sections 3 and 4), experimental setup and evaluation protocols (Section 5), and quantitative/qualitative comparisons (Tables 1–4). Additional implementation details and ablation studies are included in the Appendix to further support reproducibility. While our source code and pretrained models will be released publicly upon acceptance, the information provided in the manuscript and appendix should enable independent researchers to reproduce our findings.

REFERENCES

Michael S Albergo and Eric Vanden-Eijnden. Building normalizing flows with stochastic interpolants. *arXiv preprint arXiv:2209.15571*, 2022.

Yunpeng Bai, Cairong Wang, Shuzhao Xie, Chao Dong, Chun Yuan, and Zhi Wang. Textir: A simple framework for text-based editable image restoration. *arXiv preprint arXiv:2302.14736*, 2023.

Tim Brooks, Aleksander Holynski, and Alexei A Efros. Instructpix2pix: Learning to follow image editing instructions. In *Proceedings of the IEEE/CVF Conference on Computer Vision and Pattern Recognition*, pp. 18392–18402, 2023.

Bolun Cai, Xiangmin Xu, Kui Jia, Chunmei Qing, and Dacheng Tao. Dehazenet: An end-to-end system for single image haze removal. *IEEE transactions on image processing*, 25(11):5187–5198, 2016.

I Chen, Wei-Ting Chen, Yu-Wei Liu, Yuan-Chun Chiang, Sy-Yen Kuo, Ming-Hsuan Yang, et al. Unirestore: Unified perceptual and task-oriented image restoration model using diffusion prior. In *Proceedings of the Computer Vision and Pattern Recognition Conference*, pp. 17969–17979, 2025.

Liangyu Chen, Xiaojie Chu, Xiangyu Zhang, and Jian Sun. Simple baselines for image restoration. In *European conference on computer vision*, pp. 17–33. Springer, 2022.

Wei-Ting Chen, Hao-Yu Fang, Cheng-Lin Hsieh, Cheng-Che Tsai, I Chen, Jian-Jiun Ding, Sy-Yen Kuo, et al. All snow removed: Single image desnowing algorithm using hierarchical dual-tree complex wavelet representation and contradict channel loss. In *Proceedings of the IEEE/CVF International Conference on Computer Vision*, pp. 4196–4205, 2021.

Yu-Wei Chen and Soo-Chang Pei. Always clear days: Degradation type and severity aware all-in-one adverse weather removal. *arXiv preprint arXiv:2310.18293*, 2024.

Marcos V Conde, Gregor Geigle, and Radu Timofte. Instructir: High-quality image restoration following human instructions. In *European Conference on Computer Vision*, pp. 1–21. Springer, 2025.

Yuning Cui, Syed Waqas Zamir, Salman Khan, Alois Knoll, Mubarak Shah, and Fahad Shahbaz Khan. Adair: Adaptive all-in-one image restoration via frequency mining and modulation. In *International Conference on Learning Representations*, 2025.

Xueyang Fu, Jiabin Huang, Xinghao Ding, Yinghao Liao, and John Paisley. Clearing the skies: A deep network architecture for single-image rain removal. *IEEE Transactions on Image Processing*, 26(6):2944–2956, 2017.

Yu Guo, Yuan Gao, Yuxu Lu, Huilin Zhu, Ryan Wen Liu, and Shengfeng He. Onerestore: A universal restoration framework for composite degradation. *arXiv preprint arXiv:2407.04621*, 2024.

Martin Heusel, Hubert Ramsauer, Thomas Unterthiner, Bernhard Nessler, and Sepp Hochreiter. Gans trained by a two time-scale update rule converge to a local nash equilibrium. *Advances in neural information processing systems*, 30, 2017.

Jonathan Ho, Ajay Jain, and Pieter Abbeel. Denoising diffusion probabilistic models. *Advances in neural information processing systems*, 33:6840–6851, 2020.

JiaKui Hu, Lujia Jin, Zhengjian Yao, and Yanye Lu. Universal image restoration pre-training via degradation classification. *arXiv preprint arXiv:2501.15510*, 2025.

Yitong Jiang, Zhaoyang Zhang, Tianfan Xue, and Jinwei Gu. Autodir: Automatic all-in-one image restoration with latent diffusion. In *European Conference on Computer Vision*, pp. 340–359. Springer, 2024.

Junjie Ke, Qifei Wang, Yilin Wang, Peyman Milanfar, and Feng Yang. Musiq: Multi-scale image quality transformer. In *Proceedings of the IEEE/CVF international conference on computer vision*, pp. 5148–5157, 2021.

Xiangtao Kong, Chao Dong, and Lei Zhang. Towards effective multiple-in-one image restoration: A sequential and prompt learning strategy. *arXiv preprint arXiv:2401.03379*, 2024.

Alex Krizhevsky, Ilya Sutskever, and Geoffrey E Hinton. Imagenet classification with deep convolutional neural networks. *Advances in neural information processing systems*, 25, 2012.

Boyi Li, Xiulian Peng, Zhangyang Wang, Jizheng Xu, and Dan Feng. Aod-net: All-in-one dehazing network. In *Proceedings of the IEEE international conference on computer vision*, pp. 4770–4778, 2017.

Boyi Li, Wenqi Ren, Dengpan Fu, Dacheng Tao, Dan Feng, Wenjun Zeng, and Zhangyang Wang. Benchmarking single-image dehazing and beyond. *IEEE transactions on image processing*, 28(1): 492–505, 2018.

Boyun Li, Yuanbiao Gou, Jerry Zitao Liu, Hongyuan Zhu, Joey Tianyi Zhou, and Xi Peng. Zero-shot image dehazing. *IEEE Transactions on Image Processing*, 29:8457–8466, 2020a.

Ruoteng Li, Loong-Fah Cheong, and Robby T Tan. Heavy rain image restoration: Integrating physics model and conditional adversarial learning. In *Proceedings of the IEEE/CVF conference on computer vision and pattern recognition*, pp. 1633–1642, 2019.

Ruoteng Li, Robby T Tan, and Loong-Fah Cheong. All in one bad weather removal using architectural search. In *Proceedings of the IEEE/CVF conference on computer vision and pattern recognition*, pp. 3175–3185, 2020b.

Zilong Li, Yiming Lei, Chenglong Ma, Junping Zhang, and Hongming Shan. Prompt-in-prompt learning for universal image restoration. *arXiv preprint arXiv:2312.05038*, 2023.

Jingyun Liang, Jiezhang Cao, Guolei Sun, Kai Zhang, Luc Van Gool, and Radu Timofte. Swinir: Image restoration using swin transformer. In *Proceedings of the IEEE/CVF international conference on computer vision*, pp. 1833–1844, 2021.

Yaron Lipman, Ricky TQ Chen, Heli Ben-Hamu, Maximilian Nickel, and Matt Le. Flow matching for generative modeling. *arXiv preprint arXiv:2210.02747*, 2022.

Shuaizheng Liu, Jianqi Ma, Lingchne Sun, Xiangtao Kong, and Lei Zhang. Instructrestore: Region-customized image restoration with human instructions. *ArXiv*, 2025.

Xingchao Liu, Chengyue Gong, and Qiang Liu. Flow straight and fast: Learning to generate and transfer data with rectified flow. *arXiv preprint arXiv:2209.03003*, 2022.

Yun-Fu Liu, Da-Wei Jaw, Shih-Chia Huang, and Jenq-Neng Hwang. Desnownet: Context-aware deep network for snow removal. *IEEE Transactions on Image Processing*, 27(6):3064–3073, 2018.

Ziwei Luo, Fredrik K Gustafsson, Zheng Zhao, Jens Sjölund, and Thomas B Schön. Controlling vision-language models for universal image restoration. *arXiv preprint arXiv:2310.01018*, 3(8), 2023a.

Ziwei Luo, Fredrik K Gustafsson, Zheng Zhao, Jens Sjölund, and Thomas B Schön. Image restoration with mean-reverting stochastic differential equations. *arXiv preprint arXiv:2301.11699*, 2023b.

Anish Mittal, Rajiv Soundararajan, and Alan C Bovik. Making a "completely blind" image quality analyzer. *IEEE Signal processing letters*, 20(3):209–212, 2012.

Guy Ohayon, Tomer Michaeli, and Michael Elad. Posterior-mean rectified flow: Towards minimum mse photo-realistic image restoration. *arXiv preprint arXiv:2410.00418*, 2024.

Ozan Özdenizci and Robert Legenstein. Restoring vision in adverse weather conditions with patch-based denoising diffusion models. *IEEE transactions on pattern analysis and machine intelligence*, 2023.

Vaishnav Potlapalli, Syed Waqas Zamir, Salman Khan, and Fahad Shahbaz Khan. Promptir: Prompting for all-in-one blind image restoration. In *Advances in Neural Information Processing Systems*, 2023.

Alec Radford, Jong Wook Kim, Chris Hallacy, Aditya Ramesh, Gabriel Goh, Sandhini Agarwal, Girish Sastry, Amanda Askell, Pamela Mishkin, Jack Clark, Gretchen Krueger, and Ilya Sutskever. Learning transferable visual models from natural language supervision. In *International conference on machine learning*, 2021.

Sudarshan Rajagopalan and Vishal M. Patel. Awracle: All-weather image restoration using visual in-context learning. In *Proceedings of the AAAI Conference on Artificial Intelligence*, 2025.

Yang Song, Jascha Sohl-Dickstein, Diederik P Kingma, Abhishek Kumar, Stefano Ermon, and Ben Poole. Score-based generative modeling through stochastic differential equations. *arXiv preprint arXiv:2011.13456*, 2020.

Yuda Song, Zhuqing He, Hui Qian, and Xin Du. Vision transformers for single image dehazing. *IEEE Transactions on Image Processing*, 32:1927–1941, 2023.

Shangquan Sun, Wenqi Ren, Xinwei Gao, Rui Wang, and Xiaochun Cao. Restoring images in adverse weather conditions via histogram transformer. In *European Conference on Computer Vision*, 2024.

Jeya Maria Jose Valanarasu, Rajeev Yasarla, and Vishal M Patel. Transweather: Transformer-based restoration of images degraded by adverse weather conditions. In *Proceedings of the IEEE/CVF Conference on Computer Vision and Pattern Recognition*, pp. 2353–2363, 2022.

A Vaswani. Attention is all you need. *Advances in Neural Information Processing Systems*, 2017.

Jianyi Wang, Kelvin CK Chan, and Chen Change Loy. Exploring clip for assessing the look and feel of images. In *Proceedings of the AAAI conference on artificial intelligence*, volume 37, pp. 2555–2563, 2023.

Tao Wang, Kaihao Zhang, Ziqian Shao, Wenhan Luo, Bjorn Stenger, Tong Lu, Tae-Kyun Kim, Wei Liu, and Hongdong Li. Gridformer: Residual dense transformer with grid structure for image restoration in adverse weather conditions. *International journal of computer vision*, 2024.

Zhou Wang, Alan C Bovik, Hamid R Sheikh, and Eero P Simoncelli. Image quality assessment: from error visibility to structural similarity. *IEEE transactions on image processing*, 13(4):600–612, 2004.

Haoning Wu, Zicheng Zhang, Erli Zhang, Chaofeng Chen, Annan Wang Liang Liao, Kaixin Xu, Chunyi Li, Jingwen Hou, Guangtao Zhai, Wenxiu Sun Geng Xue, Qiong Yan, and Weisi Lin. Q-instruct: Improving low-level visual abilities for multi-modality foundation models. In *CVPR*, 2024.

Haoning Wu, Hanwei Zhu, Zicheng Zhang, Erli Zhang, Chaofeng Chen, Liang Liao, Chunyi Li, Annan Wang, Wenxiu Sun, Qiong Yan, et al. Towards open-ended visual quality comparison. In *European Conference on Computer Vision*, pp. 360–377. Springer, 2025.

Yimin Xu, Nanxi Gao, Yunshan Zhong, Fei Chao, and Rongrong Ji. Unified-width adaptive dynamic network for all-in-one image restoration. *arXiv preprint arXiv:2401.13221*, 2024.

Hao Yang, Liyuan Pan, Yan Yang, and Wei Liang. Language-driven all-in-one adverse weather removal. In *Proceedings of the IEEE/CVF Conference on Computer Vision and Pattern Recognition*, pp. 24902–24912, 2024.

Sidi Yang, Tianhe Wu, Shuwei Shi, Shanshan Lao, Yuan Gong, Mingdeng Cao, Jiahao Wang, and Yujiu Yang. Maniqa: Multi-dimension attention network for no-reference image quality assessment. In *Proceedings of the IEEE/CVF conference on computer vision and pattern recognition*, pp. 1191–1200, 2022.

Wenhan Yang, Robby T Tan, Jiashi Feng, Jiaying Liu, Zongming Guo, and Shuicheng Yan. Deep joint rain detection and removal from a single image. In *Proceedings of the IEEE conference on computer vision and pattern recognition*, 2017.

Wenhan Yang, Wenjing Wang, Haofeng Huang, Shiqi Wang, and Jiaying Liu. Sparse gradient regularized deep retinex network for robust low-light image enhancement. In *IEEE Transactions on Image Processing*, 2021.

Tian Ye, Sixiang Chen, Jinbin Bai, Jun Shi, Chenghao Xue, Jingxia Jiang, Junjie Yin, Erkang Chen, and Yun Liu. Adverse weather removal with codebook priors. In *Proceedings of the IEEE/CVF International Conference on Computer Vision*, pp. 12653–12664, 2023.

Zhiyuan You, Zheyuan Li, Jinjin Gu, Zhenfei Yin, Tianfan Xue, and Chao Dong. Depicting beyond scores: Advancing image quality assessment through multi-modal language models. In *European Conference on Computer Vision*, 2024.

Shizhe Zang, Ming Ding, David Smith, Paul Tyler, Thierry Rakotoarivelo, and Mohamed Ali Kaafar. The impact of adverse weather conditions on autonomous vehicles: How rain, snow, fog, and hail affect the performance of a self-driving car. *IEEE vehicular technology magazine*, 14(2):103–111, 2019.

Haijin Zeng, Xiaoming Wang, Yongyong Chen, Jingyong Su, and Jie Liu. Vision-languagegradientdescent-drivenall-in-onedeepunfoldingnetworks. In *Proceedings of the IEEE Conference on Computer Vision and Pattern Recognition*, 2025.

Kaihao Zhang, Rongqing Li, Yanjiang Yu, Wenhan Luo, and Changsheng Li. Deep dense multi-scale network for snow removal using semantic and depth priors. *IEEE Transactions on Image Processing*, 30:7419–7431, 2021.

Richard Zhang, Phillip Isola, Alexei A Efros, Eli Shechtman, and Oliver Wang. The unreasonable effectiveness of deep features as a perceptual metric. In *Proceedings of the IEEE conference on computer vision and pattern recognition*, pp. 586–595, 2018.

Ronghui Zhang, Jiongze Yu, Junzhou Chen, Guofa Li, Liang Lin, and Danwei Wang. A prior guided wavelet-spatial dual attention transformer framework for heavy rain image restoration. *IEEE Transactions on Multimedia*, 2024.

Dian Zheng, Xiao-Ming Wu, Shuzhou Yang, Jian Zhang, Jian-Fang Hu, and Wei-Shi Zheng. Selective hourglass mapping for universal image restoration based on diffusion model. In *Proceedings of the IEEE/CVF conference on computer vision and pattern recognition*, 2024.

Han Zhou, Wei Dong, Xiaohong Liu, Shuaicheng Liu, Xiongkuo Min, Guangtao Zhai, and Jun Chen. Glare: Low light image enhancement via generative latent feature based codebook retrieval. In *European Conference on Computer Vision*, 2024.

Han Zhou, Wei Dong, Xiaohong Liu, Yulun Zhang, Guangtao Zhai, and Jun Chen. Low-light image enhancement via generative perceptual priors. In *Proceedings of the AAAI Conference on Artificial Intelligence*, 2025.

Yixuan Zhu, Wenliang Zhao, Ao Li, Yansong Tang, Jie Zhou, and Jiwen Lu. Flowie: Efficient image enhancement via rectified flow. In *Proceedings of the IEEE/CVF Conference on Computer Vision and Pattern Recognition*, pp. 13–22, 2024.

Yurui Zhu, Tianyu Wang, Xueyang Fu, Xuanyu Yang, Xin Guo, Jifeng Dai, Yu Qiao, and Xiaowei Hu. Learning weather-general and weather-specific features for image restoration under multiple adverse weather conditions. In *Proceedings of the IEEE/CVF conference on computer vision and pattern recognition*, pp. 21747–21758, 2023.

A Appendix

A.1 Related Works

Learning-based Adverse Weather Removal While single-weather removal excels in precision, it lacks versatility needed to handle real-world situations with multiple and complex weather conditions. To address this, blind or non-blind all-in-one models for adverse weather removal emerged. All-in-one (Li et al., 2020b), one of the earliest non-blind networks, adopts a CNN with task-specific encoders found via NAS. Zhu *et al.* (Zhu et al., 2023) then use a two-stage strategy that learns weather-general and weather-specific priors with a UNet backbone for blind weather removal. Adopting the Transformer (Vaswani, 2017), TransWeather (Valanarasu et al., 2022) matches weather-type queries to feature keys/values, while AWRCP (Ye et al., 2023) operates in latent space with codebook priors. PromptIR (Potlapalli et al., 2023) introduces plug-in prompt blocks, which use prompts to encode degradation-specific information and a prompt interaction module that dynamically guide the transformer-based restoration network. Adopting the prompt mechanism, Prompt-in-Prompt (PIP) (Li et al., 2023) learns a degradation-aware prompt and a basic restoration prompt, combining them via prompt-to-prompt and selective prompt-to-feature interactions as a plug-in module that improves multi-weather robustness. MiOIR (Kong et al., 2024) learns tasks sequentially, using prompts to reduce interference between them and to stabilize training across diverse weather conditions. U-WADN (Xu et al., 2024) adds a unified-width, nested backbone with an automatic width selector so the model focus on key points, improving efficiency in all-in-one weather removal. UtilityIR (Chen & Pei, 2024) purposes an aware of degradation type and severity model, pairing a marginal quality ranking loss with adaptive normalization/attention to tune restoration strength and handle unseen mixes. OneRestore (Guo et al., 2024) targets composite degradations by fusing scene descriptors with image features, enabling controllable restoration without assuming a single weather type. AWRaCLe Rajagopalan & Patel (2025) uses a degraded-clean context pair as a visual prompt, extracting and fusing weather and type semantics and degradation appearance cues, thus the model perceives the before–after contrast and performs targeted correction.

VLM-informed Image Restoration Language-driven image restoration models aim to use natural language to remove the effects of degradation to output a clean high-quality image. In recent years, VLM architectures achieve significant breakthroughs in language-driven image restoration tasks to guide deep learning-based models. TextIR (Bai et al., 2023) leverages CLIP (Radford et al., 2021) to guide restoration by aligning text-based description with features of the restored image. DACLIP (Luo et al., 2023a) presents a degradation-aware VLM trained on text descriptions that guides a SDE-based restoration model to learn high-quality image features. InstructPix2Pix (Brooks et al., 2023) introduces a novel diffusion-based image editing method that can modify specific features in an image based on text-based instructions. InstructIR (Conde et al., 2025) deploys human-written instructions to guide an all-in-one restoration model by feature masking. Co-Instruct (Wu et al., 2025) designs a Large multi-modality model trained on a instruction-based dataset, capable of providing detailed reasoning and answer open ended questions. VLU-Net (Zeng et al., 2025) aims at an interpretable unfolding solver whose gradient step is steered by VLM to auto-select degradation transformers, and with hierarchical feature unfolding, it delivers all-in-one restoration. LDR (Yang et al., 2024) derives a pixel-wise degradation map from natural-language queries to a VLM and uses it to route MoE experts, enabling adaptive restoration without explicit weather labels. InstructRestore (Liu et al., 2025) introduces instruction-guided, region-customized image restoration by building a dataset and a ControlNet-style model which turns natural language region descriptions into masks and per-region feature modulation.

Diffusion and Flow-based Image Restoration Modern restoration methods often base their models as stochastic differential equations (SDEs), where the forward process gradually corrupts an image with continuous time-steps of random noise. Reverse-time SDE can also be done to recover the original image. Pioneering SDE-based image restoration, Song *et al.* (Song et al., 2020) proposes a trainable neural network to approximate the score function used for correcting restoration in reverse-time SDE. IR-SDE (Luo et al., 2023b) extends prior works by replacing the standard SDE-based corruption with a mean-reverting process, providing a more true representation of image degradation types. Adopting from these works, denoising diffusion probabilistic models (Ho et al., 2020) introduce a discretized version of the SDE built on Markov chains, leading to a more simplistic and practical framework for image restoration. While SDE-based models are performant in image restoration, their inherent randomness is inefficient, requiring large number of small time-steps for accurate results. To address this, Song *et al.* (Song et al., 2020) further show that reverse-time SDE can be expressed as a probability flow ordinary differential equation (ODE), an efficient alternative that deterministically generates transport mappings via velocity fields to reverse noise. However, ODE-based models are often expensive and slow in practice as most solutions relied on simulating ODE trajectories. Flow matching (FM) (Lipman et al., 2022) is introduced as a simulation-free method that learns transport mappings with a trained neural network. To further build upon FM, Rectified flow (RF) (Liu et al., 2022) is proposed as a more simplistic solution using linear transport paths for noise-data pairs, achieving similar performance at reduced computational cost. Extending from RF, FlowIE (Zhu et al., 2024) uses linear many-to-one transport mappings instead of one-to-one noise-data pairs for strong performance across different restoration tasks. PMRF (Ohayon et al., 2024)

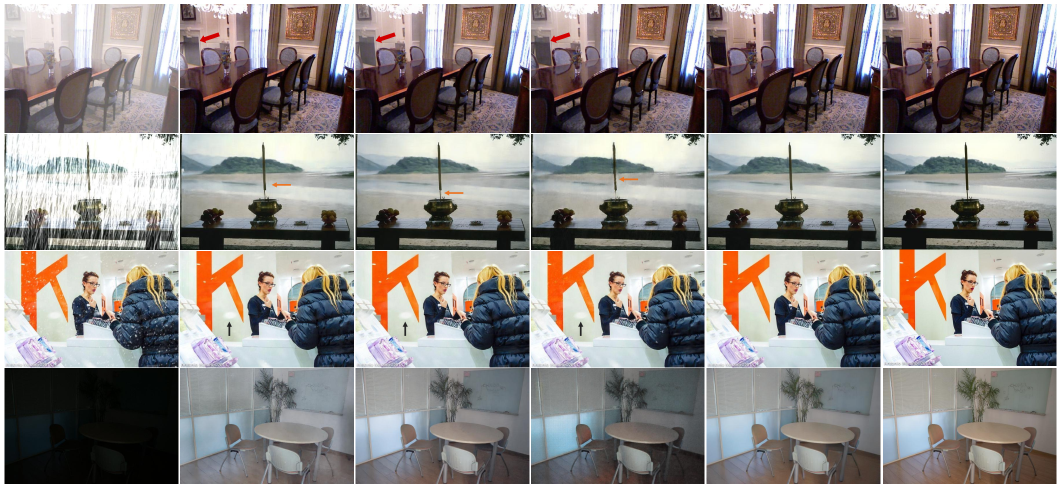

Figure 8: Visual comparisons on setting II. Previous methods often leave residual degradations or introduce artifacts (red, orange, and black arrows), whereas our RectiWeather restores clearer structures, sharper details, and more natural colors, closely matching the ground truth.

Table 6: Ablations on AWR-QA, AMN, and WWA on setting I.

Configurations	PSNR	SSIM	FID	MUSIQ
Full RectiWeather	30.37	0.932	10.46	63.12
Variant 1	28.48	0.920	13.78	62.49
Variant 2	29.53	0.928	11.78	62.77
Variant 3	29.74	0.930	11.31	62.92

uses rectified flow to approximate the optimal transport map, moving posterior mean predictions towards the ground-truth for high-quality image restoration.

A.2 Ablation Study

To analyze the contribution of each component in our method, we conduct extensive ablation studies on setting I.

AWR-specific Question Answering, Attribute-Modulated Normalization, and Weather-weighted Adapters To study the importance of our proposed AWR-specific QA and LPP-Attn, we remove these components from RectiWeather and denote the remaining network as Variant 1. Essentially, vanilla AdaIR serves as the posterior estimator in this setting, and Tab. 6 reports the average quantitative performance of Variant 1 on Setting I. Compared with Variant 1, the full RectiWeather shows significantly improved PSNR and FID by integrating soft VLM perceptions via our Attribute-Modulated Normalization and Weather-Weighted Adapters. In addition, we introduce Variant 2, which employs only the attribute perceptions, and Variant 3, which employs only the weather perceptions. These comparisons demonstrate that the two types of perceptions work complementarily to yield enhanced performance

Perception-aware Rectified Flow As reported in Tab. 7, we implement several adaptations to illustrate the importance of the source distribution built upon soft perceptions and the perception-aware velocity estimation. We observe that, if no noise is added to $\mathbf{x}_0$, RF tends to learn a deterministic flow path, while the perceptual metrics do not increase much. When the noise level is fixed, fidelity drops markedly, as evidenced by a heavy decrease in PSNR and SSIM. We observe similar behavior when a vanilla transformer backbone, without the guidance of VLM perceptions, also struggles to find the optimal flow map.

Table 7: Ablations on perception-aware rectified flow on setting I.

Configurations	PSNR	SSIM	FID	MUSIQ
Full RectiWeather	30.37	0.932	10.46	63.12
No Noise	29.24	0.927	14.27	61.88
Fix Noise Level (0.1)	28.27	0.920	14.55	61.75
w/o perceptions in f_θ	28.58	0.922	14.44	61.87

A.3 LLM USAGE

Large Language Models (LLMs) were exclusively used for language refinement such as improving grammar, clarity, and flow of the manuscript. Ideas, methodologies, experiments, and analysis were fully carried out by the authors.